URANS simulation of a realistic road vehicle with k-w SST and SSG/LRR-w model as turbulence closure

P.M Kumar, Emmanuel Guilmineau

Fourth international conference in numerical and experimental aerodynamics of road vehicles and trains (Aerovehicles4), Berlin, Germany, August 24-26, 2020

Aerovehicles 4-2020-xxxx

URANS simulation of a realistic road vehicle with k-ω SST and SSG/LRR-ω model as turbulence closure

PM. Kumar and E. Guilmineau
Corresponding author: emmanuel.guilmineau@ec-nantes.fr

LHEEA, CNRS UMR 6598, Ecole Centrale de Nantes
1 rue de la Noë, BP 92101, 44321 Nantes Cedex 3, France.

Abstract: This study discusses the comparison of numerical simulations of a realistic road vehicle using the unsteady Reynolds-averaged Navier-Stokes (URANS) with k-ω SST and SSG/LRR-ω as the turbulence closure. The ISIS-CFD solver was used to perform the simulations. A detailed grid convergence study was performed and the grid convergence index was calculated to assess the numerical uncertainty. Additionally, the flow-field of the different turbulence models were compared and reported.

Keywords: External aerodynamics, road vehicles, URANS, SSG/LRR-ω, Turbulence models.

1 Introduction

The automotive industry contributes significantly to global emissions. According to the Paris agreement, a reduction of 1.5°C in the global temperature is necessary to avoid the catastrophic effects of global warming [1]. Whereas, domestic transport accounts for about 22% of the total greenhouse gas emission in the European Union for the year 2018 [2]. The aerodynamic drag reduction of the vehicles aids in minimizing fuel consumption and it can be achieved by employing active and passive flow control methods to reduce the drag [3].

A majority of the above-mentioned studies were performed on a generic model called Ahmed body, as it consumes less computational power to perform the numerical simulations. However, owing to its simplified geometry, the obtained flow field differs from the actual flow field of the realistic vehicle. Conversely, a more realistic model such as the DrivAer has been proposed and studied to understand the actual flow behaviour of the vehicle [4]. In the present study, a realistic model of the Citroen C4 Coupe is used for the numerical analysis, and the geometry of the model is provided in Figure 1. The length (L), width (W), and height (H) of the model are 1074, 437, and 311 mm respectively and the ground clearance (G) between the C4 underbody and the bottom wall is fixed as 47.55 mm.

The computational flow domain was discretized with unstructured hexahedral elements using the Hexpress grid generator. Additionally, viscous layers are generated on the C4 surface and the bottom wall to resolve the near-wall flow physics. The ISIS-CFD solver is employed to perform the numerical simulations. It is a finite volume method based solver, developed by CNRS and Centrale Nantes and integrated with the Numeca Fine/Marine software suite. It has proved capabilities to simulate a problem using a wide range of turbulence models such as Spallart-Allmaras, k-ω, k-ω SST, Reynolds stress models (RSM) as SSG/LRR-ω, and hybrid RANS-LES, etc.

In the present work, a realistic model of the Citroen C4 Coupe is numerically studied using unsteady Reynolds-Averaged Navier-Stokes (URANS) with k-ω SST and SSG/LRR-ω as turbulence closure models. The results of the two turbulence models were compared and reported.

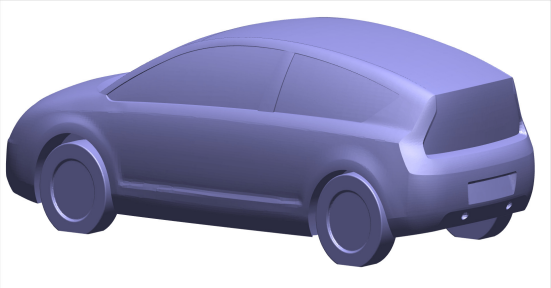

Figure 1: Citroen C4 Coupe model.

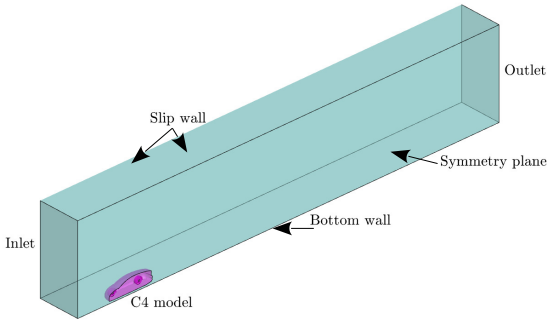

Figure 2: Computational flow domain.

2 Grid generation and convergence study

Half geometry of C4 with a symmetry boundary condition is chosen as the computational flow domain to reduce the computational cost (Figure 2). The upstream and the downstream length of the computational flow domain was kept as 6.0H and 27.6H respectively. The Hexpress grid generator was used to generate the mesh for the numerical study. The flow domain was discretized with unstructured hexahedral elements and the viscous layers were generated on the C4 surface and the bottom wall to resolve the boundary layer. Additionally, four refinement regions were added to the flow domain to facilitate better wake prediction (Figure 3). Regarding the boundary conditions, a uniform velocity of 40 m/s and zero gauge pressure were applied at the inlet and outlet, respectively. The side and top walls were kept as slip walls and a no-slip boundary was imposed on the C4 model and the bottom wall. Lastly, the symmetry plane was provided with a symmetry boundary condition and a timestep of 2.5E-4s is used for all the grids.

No. of elements in Fine/Medium/Coarse mesh, N (Million cells)	N_1 /N_2 /N_3	50.188/ 29.707/ 13.047
Performance parameter, ϕ (Average Cd) (-)	ϕ_1 , ϕ_2 , ϕ_3	0.2960/ 0.2953/ 0.2922
Characteristic length scale of the mesh, h *(m)*	h_1 /h_2 /h_3	0.00271/ 0.00323/ 0.00425
Grid refinement factor, r (-)	r_{21} , r_{32}	1.191, 1.316
Apparent order of convergence	p	5.88
Extrapolated values, Φ_{ext}	${\Phi^{21}}_{ext}$, ${\Phi^{32}}_{ext}$	0.29639, 0.29607
Approximate relative error, e_a	${e^{21}}_a$, ${e^{32}}_a$	0.00236, 0.01050
Extrapolated relative error, e_{ext}	${e^{21}}_{ext}$, ${e^{32}}_{ext}$	0.00132, 0.00261
Grid convergence index, GCI (%)	${GCI^{21}}_{fine}$, ${GCI^{32}}_{medium}$	0.165, 0.327

Table 1: Uncertainty assessment (Cd)

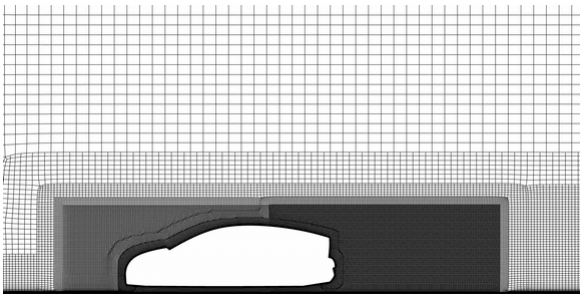

Figure 3: Enlarged view of mesh at plane Y=0.

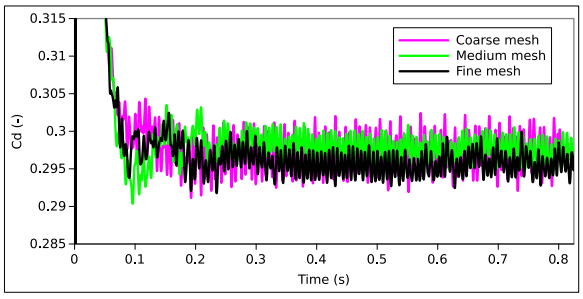

Figure 4: Drag coefficient (Cd) for various grids.

The averaged drag coefficient (Cd) values obtained from the unsteady simulations with the SSG/LRR-ω turbulence model were used for the grid convergence index (GCI) calculation. The refinement of grids was performed systematically for all grids as recommended by the work of Celik et al. [5]. The uncertainty due to

the discretization error of the Cd was provided in Table 1. As shown in Table 1, the value of GCI decreases with the increase in the grid resolution, and the obtained GCI values of the medium and the fine grids were 0.327% and 0.165% respectively. As the GCI value of the medium grid is less than 1%, it can be assumed that the spatial convergence has been achieved in the present problem and the results of medium grid were used for the comparison of the different turbulence models. Additionally, the obtained average y^+ value on the C4 surface for the coarse, medium, and fine gird was 0.255, 0.196, and 0.158 respectively. The evolution of Cd with time for different grids is shown in Figure 4.

3 Results and discussion

The comparison of Cd values for the k-ω SST and SSG/LRR-ω turbulence models are shown in Table 2. It can be observed that the variation of the Cd values between the k-ω SST and SSG/LRR-ω turbulence models decraeses with an increase in the grid resolution.

	k-ω SST	SSG/LRR-ω	Percent variation (%)
Coarse mesh	0.2974	0.2922	1.7485
Medium mesh	0.2975	0.2953	0.7395
Fine mesh	0.2959	0.2960	-0.0338

Table 2: Cd value for k-ω SST and SSG/LRR-ω turbulence models

The pressure coefficient (Cp) distribution along the surface of C4 at Y = 0 plane is provided in Figure 5. It can be seen that the SSG/LRR-ω model predicts a higher minimum suction value compared to the k-ω SST model. The Figures 6a and 6b show the streamlines of the mean flow for the different turbulence models. To compare the two cases, the limit of the recirculation bubble along with the position of recirculation centers is provided in Figure 6c. The limit of recirculation bubble obtained from the SSG/LRR-ω and k-ω SST models were almost identical. However, the location of recirculation centers show a significant variation between the two turbulence models. Moreover, the non-dimensional mean velocity field at X/H = 0.032 is provided in Figure 7. The wake field behind the C4 shows significant variation between the SSG/LRR-ω and k-ω SST models. A more detailed flow field analyses will be reported including the results of detached delayed eddy simulations will be included in the final version of the paper.

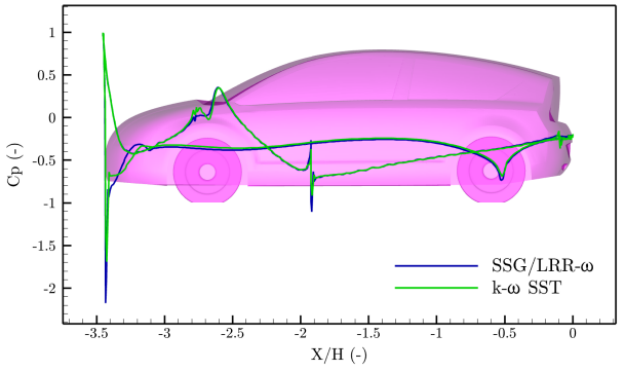

Figure 5: Mean Cp distribution on C4 surface at Y=0 plane.

4 Acknowledgement

The computations were performed using HPC resources from GENCI (Grand Equipement National de Calcul Intensif) (Grant-A0082A00129, Grant-A0102A00129) which is gratefully acknowledged. This work was

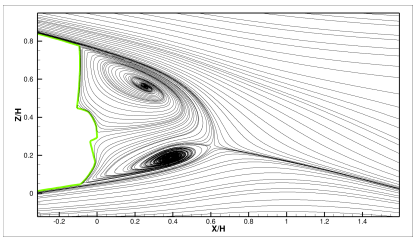

(a) SSG/LRR-ω

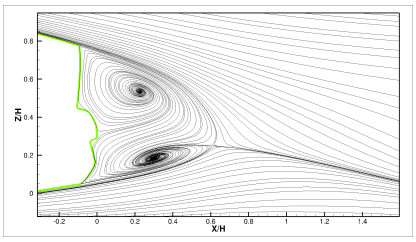

(b) k-ω SST

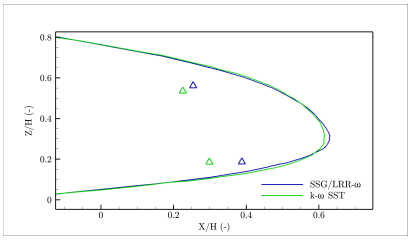

(c) Limit of recirculation bubble with centre

Figure 6: Streamlines of mean flow behind the C4 at Y = 0 plane

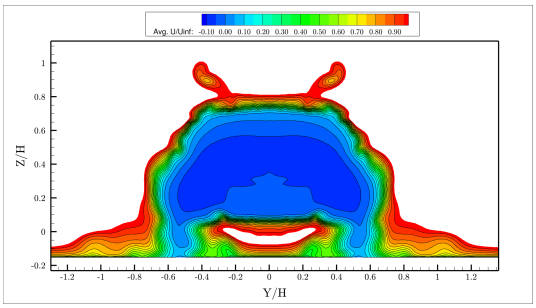

(a) SSG/LRR-ω

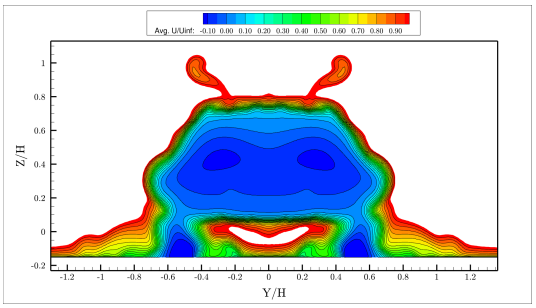

(b) k-ω SST

Figure 7: Non-dimensional mean velocity field at X/H = 0.032.

supported by the French by the French National Research Agency (ANR) through the COWAVE project (ANR-17-CE22-0008-01).

References

[1] IPCC, 2018: Summary for Policymakers. In *Global Warming of 1.5°C.* An IPCC Special Report on the impacts of global warming of 1.5°C above pre-industrial levels and related global greenhouse gas emission pathways, in the context of strengthening the global response to the threat of climate change, sustainable development, and efforts to eradicate poverty.

[2] M. Pichler, N. Krenmayr, E. Schneider, and U. Brand. EU industrial policy: Between modernization and transformation of the automotive industry. *Environmental Innovation and Societal Transitions*, 38:140–152, 2021.

[3] C.H. Bruneau, E. Creuse, D. Depeyras, P. Gillieron, and I. Mortazavi. Coupling active and passive techniques to control the flow past the square back ahmed body. *Computers & Fluids*, 39(10):1875–1892, 2010.

[4] D. Wieser, C.N. Nayeri, and C.O. Paschereit. Wake structures and surface patterns of the drivaer notchback car model under side wind conditions. *Energies*, 13(2):320, 2020.

[5] I.B. Celik, U. Ghia, P.J. Roache, and C.J. Freitas. Procedure for estimation and reporting of uncertainty due to discretization in cfd applications. *Journal of Fluids Engineering*, 130(7):078001, 2008.